

# Design of an Adaptive Gust Response Alleviation Control System: Simulations and Experiments

Ke Shao,\* Zhigang Wu,† Chao Yang,‡ and Lei Chen§

Beijing University of Aeronautics and Astronautics, 100191 Beijing, People's Republic of China  
and  
Bin Lv¶

No. 203 Research Institute of China Ordnance Industries,  
710065 Xi'an, People's Republic of China

DOI: 10.2514/1.46689

An adaptive gust response alleviation control system based on fuzzy logic was designed for a large-aspect-ratio and two-control-surface wing model. A state-space model consisting of an elastic wing model, an actuator segment, and a gust segment was established. Time-domain and frequency-domain simulations and analyses were conducted for continuous random gust response alleviation. Experiments and simulations of continuous sinusoidal gust response alleviation were spread out over time and frequency domains. The simulated results agree well with the experimental results. The control system effectively acts on random gusts in simulations. The control system has similar effects on sinusoidal gusts of different frequencies at different flow velocities in the experiments. The alleviation efficiency of sinusoidal gusts is higher than the alleviation efficiency of random gusts, while the range of the wing-tip gust response is the same.

## Nomenclature

$A_0, B_0, C_0,$ $D_0, E_0, F_0$	= state-space matrices
$a$	= modifying factor, defined in Eq. (15), $a \in [0, 1]$
$b$	= one-half reference chord
$C$	= generalized damping matrix
$D$	= matrix shown in Eq. (3)
$E_q, E_\delta, E_g$	= matrices shown in Eq. (3)
$f$	= generalized aerodynamic force
$G$	= amplitude of normal gust velocity
$g$	= unit gravitational acceleration, 9.8 m/s <sup>2</sup>
$I$	= unit matrix
$K$	= generalized stiffness matrix
$k_i$	= related coefficient of integral $y_{ac}$ , defined in Eq. (14)
$k_{i0}$	= deflection of control surface per unit acceleration response integration, defined in Eq. (15)
$k_p$	= related coefficient of $y_{ac}$ , defined in Eq. (14)
$k_{p0}$	= deflection of control surface per unit acceleration response, defined in Eq. (15)
$L$	= gust dimension
$M$	= generalized mass matrix
$M_\delta$	= coupling inertial mass caused by $\delta$
$p$	= nondimensionalized Laplace variable, $sb/v$
$Q_0$	= generalized aerodynamic force matrix

$q, \dot{q}, \ddot{q}$	= generalized coordinates
$R$	= matrix
$r$	= gust response alleviation efficiency, defined in Eq. (16)
$s$	= Laplace transform variable
$t$	= time variable
$u_{ac}$	= vector of control-surface deflections
$u_c$	= commanded control-surface deflections
$v$	= flow velocity
$w_{ae}$	= normal vector component of the gust velocities
$w_g, \dot{w}_g$	= normal component of the gust velocity
$x_a$	= hysteretic state of generalized aerodynamic force
$x_0$	= state vector
$y_{ae}$	= normal component of wing-surface acceleration response
$\delta, \dot{\delta}, \ddot{\delta}$	= control-surface deflections
$\eta$	= zero-mean-value white noise
$\rho$	= air density
$\sigma_g$	= strength of normal gust velocity
$\sigma_y()$	= root-mean-square value of $y_{ae}$ , defined in Eq. (16)
$\phi$	= mode matrix at the sensor position
$\omega_0$	= frequency

## Subscripts

ac	= actuator
ae	= elastic wing model
c	= control surface
g	= gust
q	= generalized coordinate
$\delta$	= control-surface deflection

Received 10 August 2009; revision received 26 January 2010; accepted for publication 29 January 2010. Copyright © 2010 by the American Institute of Aeronautics and Astronautics, Inc. All rights reserved. Copies of this paper may be made for personal or internal use, on condition that the copier pay the \$10.00 per-copy fee to the Copyright Clearance Center, Inc., 222 Rosewood Drive, Danvers, MA 01923; include the code 0021-8669/10 and \$10.00 in correspondence with the CCC.

\*Ph.D. Candidate, School of Aeronautic Science and Engineering; silan9@126.com.

†Associate Professor, School of Aeronautic Science and Engineering; wuzhigang@buaa.edu.cn.

‡Professor, School of Aeronautic Science and Engineering; yangchao@buaa.edu.cn.

§Ph.D. Candidate, School of Aeronautic Science and Engineering.

¶Engineer; lvbin12@163.com.

## I. Introduction

GUSTS can adversely affect large aircraft during high-speed cruising and turns. They not only cause the aircraft to produce an unexpected additional overload, but they also easily lead to vibrations and jolts that influence the maneuverability, stability, and ride quality of the aircraft. Gust alleviation and ride-quality control

have long been two of the focuses of scholarly research in active control technology for large aircraft [1–3].

Gust response can be alleviated using the following stages: the motion state of the aircraft is first detected via sensors, and control surfaces are then maneuvered, deflecting according to the control laws, and finally direct lift is produced to alleviate the gust response [4]. Gust response alleviation systems can effectively improve the flight performance of the aircraft and make the airborne apparatus work steadily. They can also improve the ride quality of the aircraft.

Many studies of gust response alleviation control laws have been conducted. A gust alleviation controller using an optimal control method was designed in [5] for a sensorcraft. In [6], a dynamic asymptotic decoupling method for a multi-input/multi-output system was proposed. A number of additional valuable studies of gust response alleviation have been published [7–11].

In the numerous investigations of gust response alleviation, adaptive control laws based on artificial intelligence theories are rare. In recent years, increasing numbers of artificial intelligence algorithms have been applied in various fields, such as electronic engineering, automation, communication, and aerospace engineering [12,13]. With respect to gust response alleviation, there is relevant research involving neural network algorithms as well [14]. Control laws based on artificial intelligence theories are more flexible than other control laws of gust response alleviation. They can allow for specific handling of different situations and are more robust. However, theoretical and relative experimental studies of gust alleviation control laws based on artificial intelligence theories have been insufficient up to now.

There are many kinds of artificial intelligence algorithms. Fuzzy logic theory has a strong adaptability to the arrangement of structures, controlling methods, and expressions, and control laws based on fuzzy logic can be easily realized in applications. Thus, an adaptive gust response alleviation control system based on fuzzy logic was designed for a large-aspect-ratio wing model in this paper. An aeroservoelastic state-space model considering the effects of actuators and gusts was established as the basis of the whole gust alleviation control system. Furthermore, a gust response alleviation control law was designed for a wing model with two control surfaces as the main body of the system. A neural network algorithm was used to obtain membership functions for the control law. Finally, simulations and experiments of this control law were conducted.

## II. Experimental Model

The experimental model was a large-aspect-ratio wing model with two control surfaces: an outer aileron and an inner aileron, as shown in Fig. 1. An acceleration transducer was assembled in the wing tip of the model. The wing had the NACA-0015 airfoil shape with a 2 m span, a 0.65 m chord at the wing root, and a 0.2 m chord at the wing tip. The leading-edge backswept angle of the wing was 20°. The root of the wing was fixed.

All tests of the large-aspect-ratio wing model were performed in the China Academy of Aerospace Aerodynamics FD-09 low-speed wind tunnel. The wind tunnel is a closed-circuit tunnel with a 3 × 3 m test section.

A gust generator device was installed at the beginning of the wind-tunnel test section (see Fig. 1). It consisted of two small wings that rotate according to the same designated frequency and amplitude about a pinned axis to produce continuous sinusoidal gusts in the test section. The gust response alleviation control law regards the wing-tip acceleration signal and flow velocity signal as inputs and the deflections of the two control surfaces as outputs to alleviate gust responses.

According to the tests, the first mode of the model is the first bending mode with a frequency of 1.6 Hz; the second mode is the second bending mode with a frequency of 6.2 Hz; the third mode is the first torsional mode with a frequency of 14.9 Hz; the flutter velocity is 35 m/s, the flutter frequency is about 9 Hz, and the associating modes are the second bending mode and the first torsional mode.

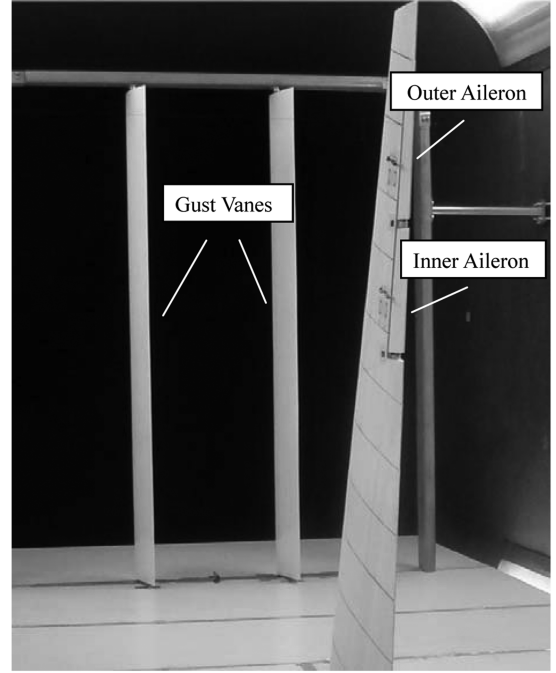


Fig. 1 Photograph of the experimental model in the wind tunnel.

## III. State-Space Model

To study gust response alleviation, a linear state-space model considering the effects of control actuators and gusts on the basis of the equations of motion of an elastic model was designed. This allowed for a comprehensive analysis of the elastic model and the control system can be carried out.

### A. State-Space Model of the Elastic Wing

The aeroelastic equation of motion in generalized coordinates is [15,16]

$$M\ddot{q} + C\dot{q} + Kq = -M_\delta\ddot{\delta} + f \quad (1)$$

where  $f$  is expressed by

$$f = \frac{1}{2}\rho v^2[\mathcal{Q}_q q + \mathcal{Q}_\delta \delta + \mathcal{Q}_g(w_g/v)] \quad (2)$$

Using the minimum state method to approximate unsteady aerodynamic forces as a rational function [1],

$$[\mathcal{Q}_q \quad \mathcal{Q}_\delta \quad \mathcal{Q}_g] = [\mathcal{Q}_{q0} \quad \mathcal{Q}_{\delta 0} \quad \mathcal{Q}_{g0}] + p[\mathcal{Q}_{q1} \quad \mathcal{Q}_{\delta 1} \quad \mathcal{Q}_{g1}] + p^2[\mathcal{Q}_{q2} \quad \mathcal{Q}_{\delta 2} \quad \mathcal{Q}_{g2}] + pD(pI - R)^{-1}[\mathcal{E}_q \quad \mathcal{E}_\delta \quad \mathcal{E}_g] \quad (3)$$

Introducing the hysteretic state of the aerodynamic force  $x_a$ ,

$$\dot{x}_a = (v/b)Rx_a + \mathcal{E}_q \dot{q} + \mathcal{E}_\delta \dot{\delta} + \mathcal{E}_g(\dot{w}_g/v) \quad (4)$$

Then we substitute Eqs. (3) and (4) in Eq. (2):

$$f = \frac{1}{2}\rho v^2 Dx_a + \frac{1}{2}\rho v^2[\mathcal{Q}_{q0} q + (b/v)\mathcal{Q}_{q1} \dot{q} + (b/v)^2 \mathcal{Q}_{q2} \ddot{q}] + \frac{1}{2}\rho v^2[\mathcal{Q}_{\delta 0} \delta + (b/v)\mathcal{Q}_{\delta 1} \dot{\delta} + (b/v)^2 \mathcal{Q}_{\delta 2} \ddot{\delta}] + \frac{1}{2}\rho v^2[\mathcal{Q}_{g0}(w_g/v) + (b/v)\mathcal{Q}_{g1}(\dot{w}_g/v) + (b/v)^2 \mathcal{Q}_{g2}(\ddot{w}_g/v)] \quad (5)$$

If we consider measuring the gust response of the wing with acceleration transducers, then

$$y_{ae} = \phi \ddot{q} \quad (6)$$

From Eqs. (1), (5), and (6), a state-space equation of the elastic wing yields

$$\begin{cases} \dot{\mathbf{x}}_{ae} = \mathbf{A}_{ae}\mathbf{x}_{ae} + \mathbf{B}_{ae}\mathbf{u}_{ae} + \mathbf{E}_{ae}\mathbf{w}_{ae} \\ \mathbf{y}_{ae} = \mathbf{C}_{ae}\mathbf{x}_{ae} + \mathbf{D}_{ae}\mathbf{u}_{ae} + \mathbf{F}_{ae}\mathbf{w}_{ae} \end{cases} \quad (7)$$

where

$$\mathbf{x}_{ae} = \begin{bmatrix} \mathbf{q} \\ \dot{\mathbf{q}} \\ \mathbf{x}_a \end{bmatrix}; \quad \mathbf{u}_{ae} = \begin{bmatrix} \delta \\ \dot{\delta} \\ \delta \end{bmatrix}; \quad \mathbf{w}_{ae} = \begin{bmatrix} \mathbf{w}_g \\ \dot{\mathbf{w}}_g \end{bmatrix}$$

### B. Actuators

The actuator is approximated with a third-order transfer function:

$$\delta/u_c = b_0/(s^3 + a_2s^2 + a_1s + a_0) \quad (8)$$

From Eq. (8), the state-space equation of the actuator yields

$$\begin{cases} \dot{\mathbf{x}}_{ac} = \mathbf{A}_{ac}\mathbf{x}_{ac} + \mathbf{B}_{ac}\mathbf{u}_c \\ \mathbf{u}_{ae} = \mathbf{C}_{ac}\mathbf{x}_{ac} \end{cases} \quad (9)$$

### C. Gusts

Two kinds of gusts were used in this study. The first was a sinusoidal gust, expressed as

$$\mathbf{w}_g = G \sin(2\pi\omega_g t) \quad (10)$$

and the other was a random gust. In general, there are two power spectrum models: the Dryden model and the von Kármán model. The Dryden model, which can be used in time-domain simulations, is an approximation of the von Kármán model when the gust frequency is low. The Dryden model is used in this paper, and the transfer function of a random gust is

$$w_g/\eta = \sigma_g \sqrt{L/\pi v} (1 + 2\sqrt{3}(L/v)s) / (1 + 2(L/v)s)^2 \quad (11)$$

From Eq. (11), the state-space equation of a random gust yields

$$\begin{cases} \dot{\mathbf{x}}_g = \mathbf{A}_g\mathbf{x}_g + \mathbf{B}_g\eta \\ \mathbf{w}_{ae} = \mathbf{C}_g\mathbf{x}_g + \mathbf{D}_g\eta \end{cases} \quad (12)$$

### D. State-Space Model of the Gust Response Alleviation System

According to Eqs. (7), (9), and (12), a state-space model of the gust response alleviation system yields

$$\begin{cases} \dot{\mathbf{x}} = \mathbf{A}\mathbf{x} + \mathbf{B}\mathbf{u}_c + \mathbf{E}\eta \\ \mathbf{y}_{ae} = \mathbf{C}\mathbf{x} + \mathbf{F}\eta \end{cases} \quad (13)$$

where

$$\mathbf{x} = \begin{bmatrix} \mathbf{x}_{ae} \\ \mathbf{x}_{ac} \\ \mathbf{x}_g \end{bmatrix}; \quad \mathbf{A} = \begin{bmatrix} \mathbf{A}_{ae} & \mathbf{B}_{ae}\mathbf{C}_{ac} & \mathbf{E}_{ae}\mathbf{C}_g \\ 0 & \mathbf{A}_{ac} & 0 \\ 0 & 0 & \mathbf{A}_g \end{bmatrix}$$

$$\mathbf{B} = \begin{bmatrix} 0 \\ \mathbf{B}_{ac} \\ 0 \end{bmatrix}; \quad \mathbf{E} = \begin{bmatrix} \mathbf{E}_{ae}\mathbf{D}_g \\ 0 \\ \mathbf{B}_g \end{bmatrix}$$

$$\mathbf{C} = [\mathbf{C}_{ae} \quad \mathbf{D}_{ae}\mathbf{C}_{ac} \quad \mathbf{F}_{ae}\mathbf{C}_g]; \quad \mathbf{F} = [\mathbf{F}_{ae}\mathbf{D}_g]$$

As shown in Eq. (5),  $\mathbf{f}$  is a nonlinear function of  $v$ ; therefore, based on Eqs. (1–13), the final state-space model shown in Eq. (13) is a nonlinear function of  $v$ .

If the gust is sinusoidal, then the state-space equation (13) will be simplified, Eq. (12) is not combined with Eq. (13), and the gust input of the state-space model is directly imported as Eq. (10). In the experiments, the bandwidth of the actuator is about 7 Hz when the control-surface deflection is  $\pm 10$  deg. According to the characteristics of the actuator, we can obtain the actuator constants in Eq. (8):  $a_0 = 330186$ ,  $a_1 = 8789$ ,  $a_2 = 127.2$ , and  $b_0 = 330186$ .

## IV. Control System Design

### A. Gust Response Alleviation System Design Scheme

The diagram of the gust response alleviation system presented in Fig. 2 is used to synthesize the controllers for the purpose of this work. The whole system is an adaptive control system with three controllers, including controller A, controller KP, and controller KI. The input of the system is the acceleration response  $\mathbf{y}_{ae}$  and airspeed  $v$ , and the output is the command of the control-surface deflections,  $\mathbf{u}_c$ , as shown in Fig. 2.

Supposing  $k_p$  to be the related coefficient of  $\mathbf{y}_{ae}$ , and  $k_i$  to be the related coefficient of  $\int d\mathbf{y}_{ae}/dt$ , then

$$\mathbf{u}_c = k_p \cdot \mathbf{y}_{ae} + k_i \cdot \int \frac{d\mathbf{y}_{ae}}{dt} \quad (14)$$

The values and proportions of  $k_p$  and  $k_i$  will exert a tremendous influence on the control system. Thus, we add a modifying factor  $a$  ( $a \in [0, 1]$ ):

$$\mathbf{u}_c = a \cdot k_{p0} \cdot \mathbf{y}_{ae} + (1 - a) \cdot k_{i0} \cdot \int \frac{d\mathbf{y}_{ae}}{dt} \quad (15)$$

According to Eq. (15), we design the control system model. In this model,  $k_{p0}$ ,  $k_{i0}$ , and  $a$  vary nonlinearly with  $\mathbf{y}_{ae}$  or  $v$ . We set up three fuzzy logic controllers, which have two inputs and one output: fuzzy logic controller A, fuzzy logic controller KP, and fuzzy logic controller KI (see Fig. 2). Therefore, the nonlinear characteristics of  $k_{p0}$ ,  $k_{i0}$ , and  $a$  can be considered through these fuzzy logic controllers.

### B. Fuzzy-Logic-Based Control Law

Generally, fuzzy subsets are used as the input and output sets in fuzzy-logic-based control laws [17]. Therefore, the sequence of operations in a fuzzy system can be described by three phases: fuzzification, inference, and defuzzification [18]. The inputs of the control system are crisp, but the input sets of the fuzzy-logic-based control laws must be fuzzy subsets. Consequently, fuzzification that converts crisp input data into fuzzy subsets through linguistic variables and their membership functions is needed. Inference is based on the fuzzy rules. Using the max min (Mamdani–Assilian type) inference [17], we can generate the best possible conclusions. In fact, this type of inference is computationally easy and effective; thus, it is appropriate for real-time control applications [18]. Defuzzification refers to the process of determining crisp output data according to the fuzzy subsets of outputs of the control law. We use the centroid-of-area defuzzification procedure to do this. The criterion provides the defuzzified output with better continuity [18].

Therefore, we need to devise the input and output linguistic variables, build up the relative membership functions, and set up the rules for the fuzzy logic controllers. These will be introduced in the following paragraphs.

The input linguistic variables of the three fuzzy logic controllers are  $\mathbf{y}_{ae}$  and  $v$ , and the output variable of the fuzzy logic controller A is

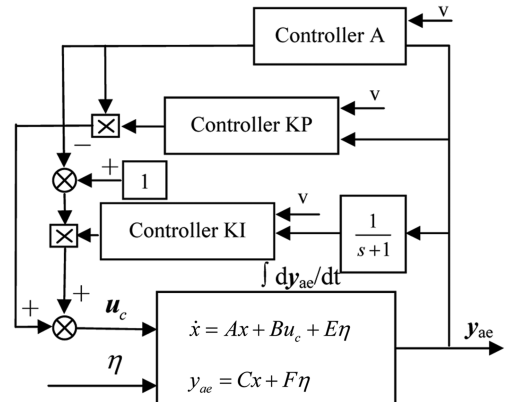


Fig. 2 Schematic diagram of the gust response alleviation system.

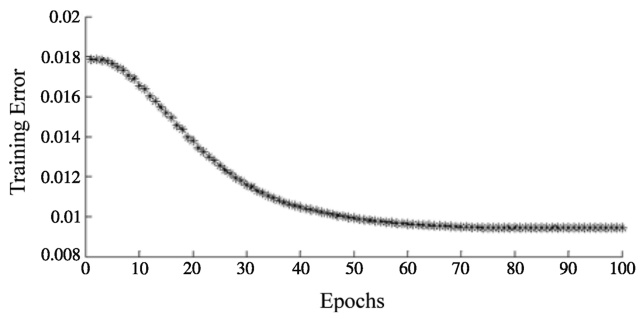
$a$ , the output variable of the fuzzy logic controller KP is  $k_{p0}$ , and the output variable of the fuzzy logic controller KI is  $k_{i0}$ .

The input variable  $y_{ae}$  is supposed to take five linguistic sets defined as NB (negative big), NS (negative small), ZO (zero), PS (positive small), and PB (positive big). The other input variable  $v$  is supposed to take six linguistic sets defined as ST (smallest), SE (smaller), M (middle), BE (bigger), BT (biggest), and FA (fatal). The output variable  $a$  is supposed to take five linguistic sets defined as ST, SE, M, BE, and BT. Finally, the output variables  $k_{p0}$  and  $k_{i0}$  are supposed to take six linguistic sets defined as ST, SE, M, BE, BT, and ZO.

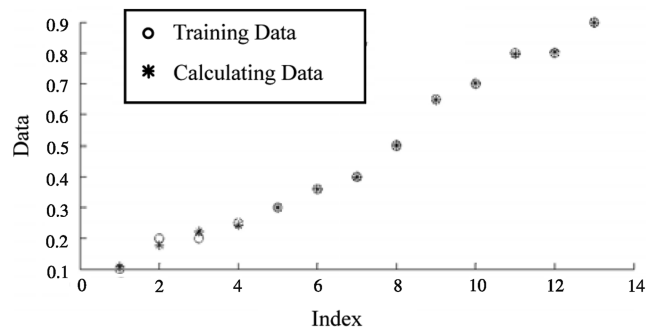
The universe of discourse of the linguistic variable  $y_{ae}$  is taken to be  $-10$  to  $10$  g, where  $g$  is the unit overload,  $g = 9.8 \text{ m/s}^2$ ,  $v$  is taken to be  $8\text{--}38 \text{ m/s}$ ,  $a$  is a dimensionless parameter, and its universe of discourse is supposed to be  $0\text{--}0.9$ . The bounds of  $k_{p0}$  and  $k_{i0}$  can be obtained through calculating the responses of  $y_{ae}$  and  $\int dy_{ae}/dt$  when inputting the step signal of  $u_c$ . In this model, the largest values of  $k_{p0}$  and  $k_{i0}$  are  $31.3$  and  $416.7$ , respectively, when  $v$  is  $8 \text{ m/s}$ . Therefore,  $k_{p0}$  is supposed to be  $0$  to  $31.3 \text{ deg/g}$ , and  $k_{i0}$  is supposed to be  $0$  to  $416.7 \text{ deg}\cdot\text{s/g}$ , where  $g = 9.8 \text{ m/s}^2$ .

The state-space model was corrected by a ground vibration test. The membership functions of the controllers can be obtained based on the state-space model using a neural network algorithm. However, the membership functions cannot be obtained from the state-space model directly, and only discrete data can be obtained. Hence, a neural network algorithm (error backpropagation algorithm) was introduced to fit the membership functions using these discrete data. To obtain the membership functions, we need to acquire three main groups of discrete data according to the state-space model: the first group presents  $k_{p0}$  varying with  $v$ , the second group presents  $k_{i0}$  varying with  $v$ , and the third group presents  $a$  varying with  $v$ . The first and second groups can be obtained through inputting the step signal of  $u_c$  to the state-space model. We must refer to simulation results of the gust response alleviation using a sequence of  $a$  to obtain the data in the third group. Other relationships between variables, e.g., relationships between  $k_{p0}$  and  $y_{ae}$ , do not show strong non-linearity. Therefore, the membership functions will be established mainly according to the three groups.

The trend of variable  $a$  varying with  $v$  using the neural network algorithm is shown in Fig. 3. The training data shown in Fig. 3 are the



a) Training error vs. epochs



b) Comparison between training data and calculating data

Fig. 3 Trend of the fitting function of variable  $a$ .

discrete data obtained according to the state-space model, and the calculating data are the data calculated according to the fitting membership functions. Figure 3a shows that the error between the fitting function and the training data is reduced as the epochs increase. Figure 3b shows a comparison between data calculated based on the trained fitting function and the training data, and the two show good agreement. The variables  $k_{p0}$  and  $k_{i0}$  are trained in the same way. Finally, all of the fuzzy subsets of the three fuzzy logic controllers are described by their membership functions, presented in Figs. 4–8. The membership functions of  $y_{ae}$  in the three fuzzy logic controllers are the same; therefore, only one membership function of  $y_{ae}$  is presented. The membership functions of  $v$  in the three controllers are the same, too. There are many forms of membership functions, e.g., Gaussian-shaped functions. However, triangular membership functions are suggested for easy computation in the actual operation.

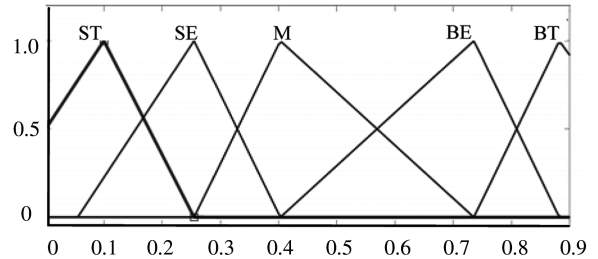


Fig. 4 Membership function of  $a$ .

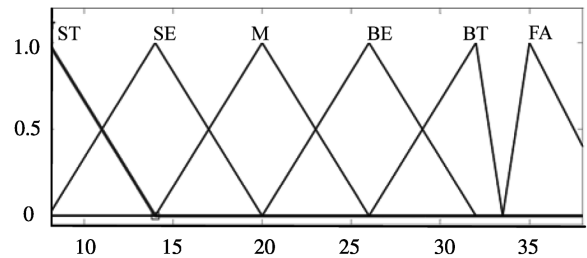


Fig. 5 Membership function of  $v$ .

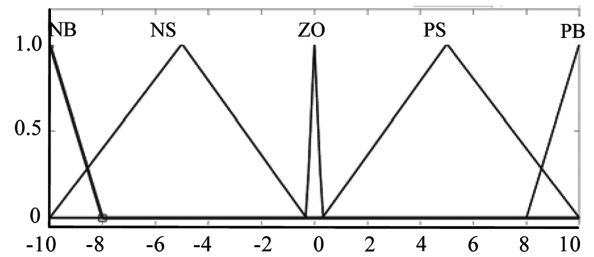


Fig. 6 Membership function of  $y_{ae}$ .

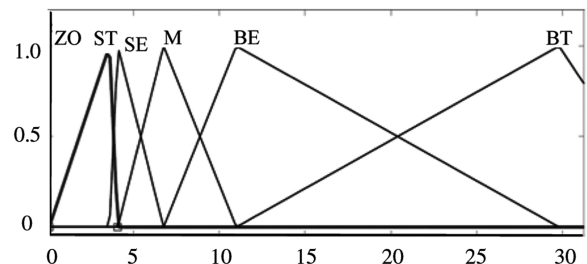


Fig. 7 Membership function of  $k_{p0}$ .

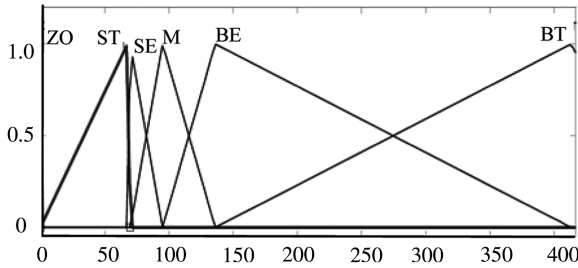


Fig. 8 Membership function of  $k_{i0}$ .

The complete rules of fuzzy logic controller A are given in Table 1. The rules of controller KP are the same as those of controller KI, as shown in Table 2.

For illustration, some sample rules are given as follows: If  $v$  is ST and  $y_{ae}$  is NB, then  $a$  is ST. If  $v$  is BE and  $y_{ae}$  is PS, then  $k_{p0}(k_{i0})$  is SE.

The set of rules of controller A (shown in Table 1) can be divided into the following three groups:

1) For groups 1 and 5,  $|y_{ae}|$  is too large, so  $a$  should be smaller than the calculated results. While  $|y_{ae}|$  is too large, the control system may overshoot, so  $a$  should be reduced, and  $k_p$  will decrease accordingly. This benefits the stability of this control system.

2) For groups 2 and 4,  $|y_{ae}|$  is in the normal range, and  $a$  should agree with the calculated results.

3) For group 3,  $|y_{ae}|$  is smaller than  $0.2g$ , and  $a$  should also agree with the calculated results.

The set of rules of controller KP (KI) (shown in Table 2) can be divided into the following four groups:

1) For groups 1 and 5,  $|y_{ae}|$  is too large and leads to a reduction in the alleviation efficiency, so  $k_{p0}(k_{i0})$  should be smaller than the calculated results. The deflections of the control surfaces were restricted in the experiments and simulations. If  $|y_{ae}|$  is too large, the deflections will go beyond the range of restrictions, and the alleviation efficiency of the control system will drop rapidly.  $k_{p0}(k_{i0})$  should be reduced at this time, and  $u_c$  will decrease accordingly; therefore, the burden on the control surfaces will be reduced, and the alleviation efficiency will increase.

2) For groups 2 and 4,  $|y_{ae}|$  is in the normal range, so  $k_{p0}(k_{i0})$  should agree with the calculated results.

3) For group 3,  $|y_{ae}|$  is smaller than  $0.2g$ , considering the noise interference, and  $k_{p0}(k_{i0})$  is set close to zero to make the control system more stable.

4) For group 6,  $v$  is close to the flutter speed, and  $k_{p0}(k_{i0})$  is set close to zero. The flutter speed of the model tested in the experiments is  $35 \text{ m/s}$ . Therefore,  $k_{p0}(k_{i0})$  is set to zero when  $v$  is greater than  $33.5 \text{ m/s}$ . Because of this rule, we can design another flutter

Table 1 Rule table for  $a$  of controller A

$y_{ae}$	$v$					
	ST	SE	M	BE	BT	FA
NB group 1	ST	ST	SE	M	BE	BE
NS group 2	ST	SE	M	BE	BT	BT
ZO group 3	ST	SE	M	BE	BT	BT
PS group 4	ST	SE	M	BE	BT	BT
PB group 5	ST	ST	SE	M	BE	BE

Table 2 Rule table for  $k_{p0}(k_{i0})$  of controller KP (KI)

$y_{ae}$	$v$					
	ST	SE	M	BE	BT	FA
NB group 1	BE	M	SE	ST	ST	ZO <sup>a</sup>
NS group 2	BT	BE	M	SE	ST	ZO <sup>a</sup>
ZO group 3	ZO	ZO	ZO	ZO	ZO	ZO <sup>a</sup>
PS group 4	BT	BE	M	SE	ST	ZO <sup>a</sup>
PB group 5	BE	M	SE	ST	ST	ZO <sup>a</sup>

<sup>a</sup>ZO in FA are in group 6.

suppression control system, and the two control systems will not influence each other.

## V. Simulations

### A. Effects of Gust Frequency for a Random Gust

The variable  $y_{ae}$  is calculated while the flow velocity is  $30 \text{ m/s}$ . According to the calculation results, the range of  $y_{ae}$  without the control system is  $-3.6$  to  $3.2 \text{ g}$ , and the range drops to  $-1.8$  to  $1.6 \text{ g}$  under the gust response alleviation control system. The range of the control-surface deflection is restricted to  $-10$  to  $10 \text{ deg}$ . Figure 9a shows the variation of the wing-tip acceleration response without the control system; Fig. 9b shows the response under the control system. Figure 10a shows the relative deflections of the outer aileron of the model, and the range is  $-5$  to  $5.8 \text{ deg}$ ; Fig. 10b shows the deflections of the inner aileron with a range of  $-3.2$  to  $3.8 \text{ deg}$ . Figure 11, in which the power spectral density changes with gust frequency, presents the frequency-domain analysis of the random gust response alleviation obtained when using the control system. In Fig. 11, the line with larger magnitude represents the open-loop results, and the line with smaller magnitude represents the closed-loop results.

The gust response alleviation efficiency is defined as

$$r = [\sigma_y(0) - \sigma_y(1)] / \sigma_y(0) \times 100\% \quad (16)$$

where  $\sigma_y(0)$  is the root-mean-square value of  $y_{ae}$  without the control system, and  $\sigma_y(1)$  is the root-mean-square value of  $y_{ae}$  under the control system.

Based on Eq. (16), the random gust response alleviation efficiency of the control system at  $30 \text{ m/s}$  is  $49.4\%$ .

According to Figs. 9–11, we find that the control system is more effective in the random gust response alleviation when the gust frequency is low. Regardless of whether the analysis is done in the time domain or frequency domain, the control system is very effective at  $30 \text{ m/s}$ . In addition, the deflections are in the range of  $-10$  to  $10 \text{ deg}$  all of the time;  $|y_{ae}|$  even rises to  $3.6g$  at some points. This occurs because the characteristics of the two control surfaces are not exactly the same, and some discrepancy between the deflections of the two control surfaces exists. The data presented in the Fuzzy-Logic-Based Control Law section are the values of the outer aileron control law. The inner aileron control law contains the same fuzzy logic controllers as the outer aileron control law, except that the range of the membership functions of  $k_{p0}$  and  $k_{i0}$  is slightly smaller than that of the outer control law.

### B. Effects of Flow Velocity for a Random Gust

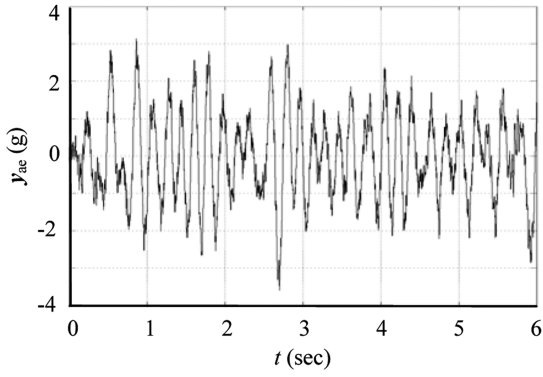
The gust response alleviation efficiency was calculated under a random gust. The range of the flow velocity is  $12$ – $30 \text{ m/s}$ . The range of the deflection is restricted to  $-10$  to  $10 \text{ deg}$ . The results are shown in Fig. 12.

According to Fig. 12, the gust response alleviation efficiency increases rapidly with the flow velocity. The alleviation efficiency reaches  $41.3\%$  at  $24 \text{ m/s}$  and  $49.4\%$  at  $30 \text{ m/s}$ . This most likely occurs because the gust response reductions are not optimal at the low flow velocities, and the reductions are close to the optimal results at the high flow velocities.

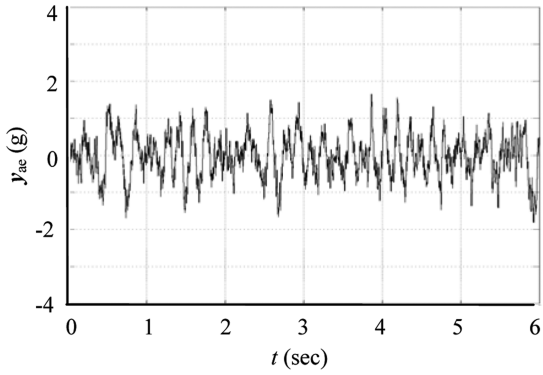
## VI. Experiments

### A. Effects of Gust Frequency for a Sinusoidal Gust

Under real conditions, most gust energy is concentrated at low frequencies. Therefore, the range of the sinusoidal gust frequency is  $2$ – $5 \text{ Hz}$  in the experiments. The range of the control-surface deflections is restricted to  $-10$  to  $10 \text{ deg}$ . The wing-tip acceleration responses under different sinusoidal gust frequencies are measured. Figure 13 shows the responses of the model when the sinusoidal gust frequency is  $2 \text{ Hz}$  and the flow velocity is  $14 \text{ m/s}$ . Figure 13a displays  $y_{ae}$  without the control system, with a range of  $-2.8$  to  $2.8 \text{ g}$ ; Fig. 13b displays  $y_{ae}$  under the control system, and the range drops to  $-2.4$  to  $2.4 \text{ g}$ .

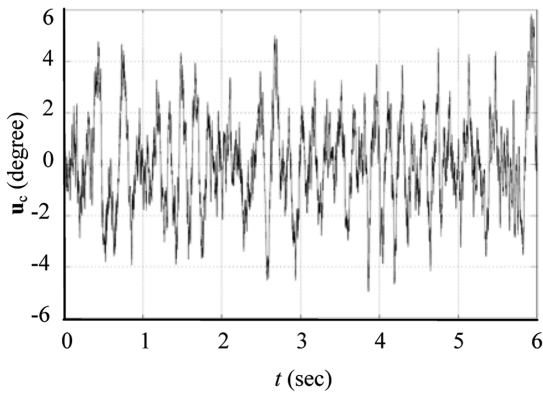


a) Open loop

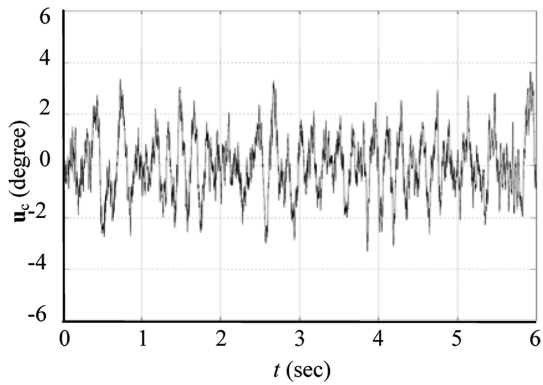


b) Closed loop

Fig. 9 Random gust response vs time.



a) Deflections of the outer aileron



b) Deflections of the inner aileron

Fig. 10 Deflections of control surfaces vs time.

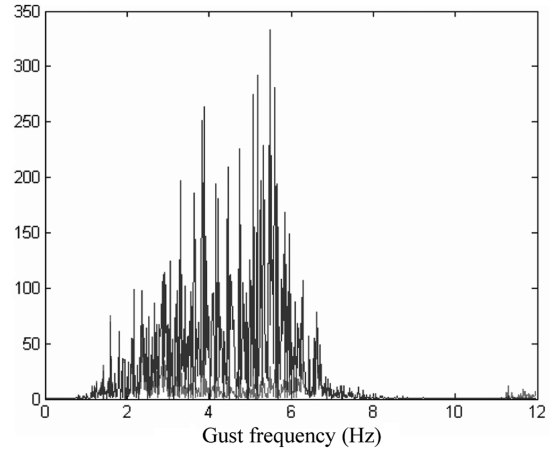


Fig. 11 Random gust response vs gust frequency.

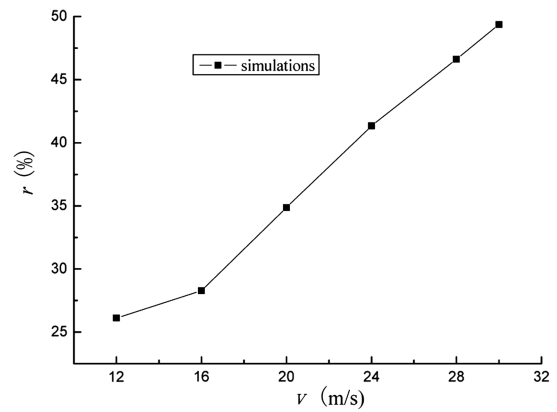
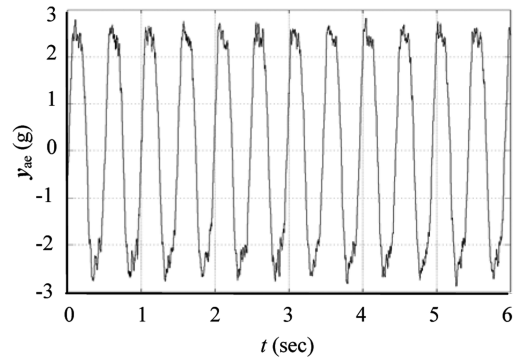
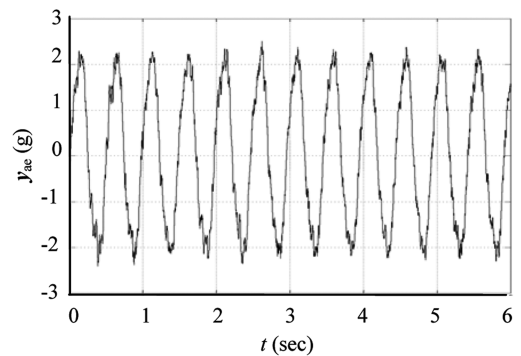


Fig. 12 Random gust response alleviation efficiency vs flow velocity.

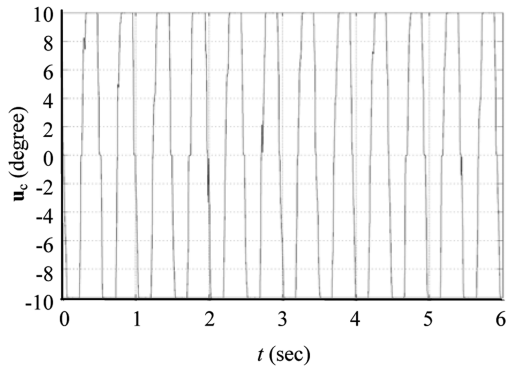


a) Open loop

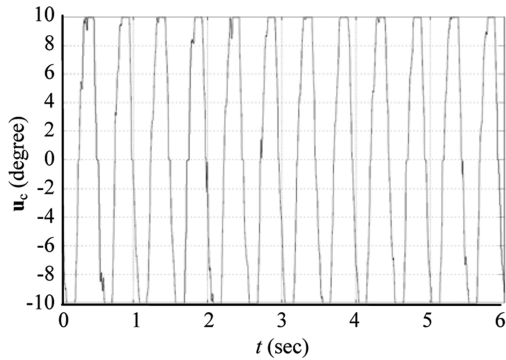


b) Close loop

Fig. 13 Sinusoidal gust response alleviation vs time.



a) Deflections of the outer aileron



b) Deflections of the inner aileron

Fig. 14 Relative deflections of control surfaces vs time.

Figure 14 shows the relative deflections of the control surfaces. Figure 14a shows the deflections of the outer aileron, and Fig. 14b shows the deflections of the inner aileron. Both of the largest deflections of the two control surfaces have reached the maximum limit.

According to Figs. 13 and 14, the gust perturbation is too great and often causes a full deflection in the experiments. This will adversely affect the alleviation effects of the control system. Nevertheless, the real perturbations of gusts will be much smaller, and the gust alleviation efficiency will be higher in reality.

The alleviation efficiency is calculated under different sinusoidal gust frequencies at the same flow velocity (14 m/s) based on the experimental data, and the alleviation efficiencies varying with the gust frequency of a sinusoidal gust are obtained, as shown in Table 3.

Table 3 Sinusoidal gust response alleviation efficiency vs gust frequency

$\omega_g$ , Hz	$\sigma_y(0)$ , g	$\sigma_y(1)$ , g	$r$
2	2.00	1.50	25.3%
2.5	1.75	1.33	24.2%
3	1.59	1.16	27.2%
3.5	1.62	1.23	24.1%
4	1.70	1.27	25.1%
4.5	1.91	1.53	19.9%
5	2.28	1.81	20.5%

Table 4 Sinusoidal gust response alleviation efficiency contrast

$\omega_g$ , Hz	$r$		$D$ value
	Experiment	Simulation	
2	25.3%	25.0%	-0.3%
2.5	24.2%	25.7%	1.5%
3	27.2%	31.8%	4.6%
3.5	24.1%	24.9%	0.8%
4	25.1%	21.4%	-3.7%
4.5	19.9%	21.5%	1.6%
5	20.5%	20.2%	-0.3%

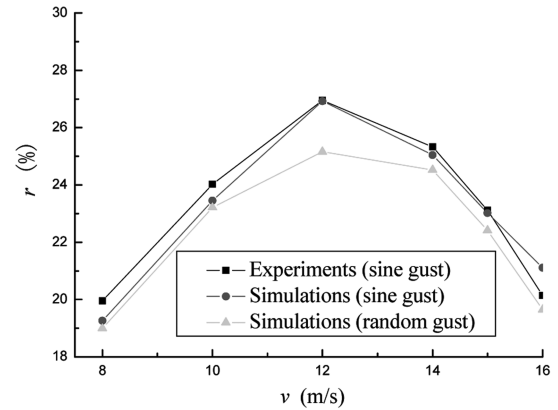


Fig. 15 Gust response alleviation efficiency contrast.

According to Table 3, using the adaptive control system, the alleviation efficiencies of sinusoidal gusts are of similar magnitudes and the range of gust frequency is 2–5 Hz.

Using the experimental uncontrolled data of  $y_{ae}$  as the input of the control system, the alleviation efficiency was calculated based on the control system model, and then the discrepancy between the experimental and simulation results was determined, as shown in Table 4. As can be seen in Table 4, the difference between the experimental and simulated results is relatively small. Hence, the simulation results of this gust alleviation control system can be regarded as effective references to experiments.

### B. Effects of Flow Velocity for a Sinusoidal Gust

The perturbation of the gust is too large in the experiments. Thus, the range of  $v$  in the experiments is restricted to 8–16 m/s. The gust alleviation efficiencies were calculated under different values of  $v$  and a fixed  $\omega_g$  of 2 Hz, based on the experimental data. Furthermore, the efficiencies for a sinusoidal gust and a random gust were calculated based on the simulation model. The experimental uncontrolled data of  $y_{ae}$  were used as one input in the sinusoidal gust alleviation simulations. In the random gust alleviation simulations, the range of  $y_{ae}$  continues to agree with the experimental uncontrolled data. The range of control-surface deflections is restricted to  $-10$  to  $10$  deg all of the time. Figure 15 presents the experimental and simulation results.

Figure 15 indicates that the experimental results have the same trend as the two simulated results. The alleviation efficiency of the random gust is lower than that of the sinusoidal gust at all flow velocities. This occurs because the random gust consists of sinusoidal gusts of different frequencies, and the alleviation efficiency varies with the sinusoidal gust frequency. Therefore, the coupling effects of different sinusoidal gusts may reduce the alleviation efficiency.

The gust alleviation efficiency reaches a maximum at 12 m/s, as shown in Fig. 15. Below 12 m/s, the efficiency increases with  $v$  because the dynamic forces acting on the control surfaces rise with  $v$ . At 12 m/s, the control-surface deflections are close to the maximum value of the restriction range. Above 12 m/s, the efficiency drops, since the perturbation of the gust is too large and the control-surface deflections are restricted. If the perturbation of the gust is smaller and the control-surface deflections remain lower than the maximum limit of the restriction range, the trend of the efficiency will be different, as shown in Fig. 12.

## VII. Conclusions

An adaptive gust response alleviation control system was designed based on fuzzy logic for a large-aspect-ratio wing model. A neural network algorithm was used to obtain the membership functions of fuzzy logic controllers. Experiments and simulations of sinusoidal gust alleviation and random gust alleviation were carried out based on this control system. The simulation results agree well with experimental results under the same gust conditions. Time-domain and frequency-domain analyses indicated that the gust response

alleviation control system has a large effect on random gusts. Gust response reductions of 20–27% were demonstrated in the experiments, and even larger reductions could be obtained at higher velocities with the same aileron displacement limits and a single wing-tip sensor. However, the reductions will decrease if the perturbation of the gust is too strong. A comparison of the experiments and simulations showed that the discrepancy in alleviation efficiency between a sinusoidal gust and a random gust is small. The control system has similar effects on both sinusoidal gusts and random gusts and is of significant value for engineering applications.

### Acknowledgment

The first author wishes to acknowledge all of the fellows in the Aeroelastic Laboratory, Beijing University of Aeronautics and Astronautics. These experiments could not have been completed without their help.

### References

- [1] Karpel, M., "Design for Active Flutter Suppression and Gust Alleviation Using State-Space Aeroelastic Modeling," AIAA Paper 80-0766, 1980.
- [2] Rennie, R. M., "Gust Alleviation using Trailing-edge Flaps," AIAA Paper 99-0649, 1999.
- [3] Mor, M., and Livne, E., "Sensitivities and Approximations for Aeroservoelastic Shape Optimization with Gust Response Constraints," AIAA Paper 2005-2077, 2005.
- [4] Liang, S. N., Wang, L. X., and Zhang, S. G., "Control Technology and Its Development of Aircraft Wing Load Alleviation," *Flight Dynamics*, Vol. 21, No. 1, 2003, pp. 1–4 (in Chinese).
- [5] Vartio, E., Shimko, A., and Tilmann, C. P., "Structural Modal Control and Gust Load Alleviation for a Sensorcraft Concept," AIAA Paper 2005-1946, 2005.
- [6] Zhang, W. G., Sun, X., Wang, W., and Li, A. J., "An Improved Gust Alleviation Method," *Journal of Northwestern Polytechnical University*, Vol. 24, No. 1, 2006, pp. 23–25 (in Chinese).
- [7] Layton, J. B., "Aeroservoelastic Tailoring for Gust Response of a Typical Section Aeroelastic Model," AIAA Paper 95-1192-CP, 1995.
- [8] Yang, C., and Zou, C. Q., "Analysis of Insensitivity to Gust for Multi-Input Aeroservoelastic System," *Acta Aeronautica et Astronautica Sinica*, Vol. 21, No. 6, 2000, pp. 496–499 (in Chinese). doi:10.3321/j.issn:1000-6893.2000.06.004
- [9] Tang, D., Gavin, H. P., and Dowell, E. H., "Theoretical-Experimental Study of Gust Alleviation Using an Electro-Magnetic Dry Friction Damper," AIAA Paper 2003-1520, 2003.
- [10] Pettit, C. L., and Grandhi, R. V., "Optimization of a Wing Structure for Gust Response and Aileron Effectiveness," *Journal of Aircraft*, Vol. 40, No. 6, 2003, pp. 1185–1191. doi:10.2514/2.7208
- [11] Karpel, M., and Moulin, B., "Aeroservoelastic Gust Response Analysis for the Design of Transport Aircrafts," AIAA Paper 2004-1529, 2004.
- [12] Zhang, G. L., Zeng, J., Ke, X. Z., and Deng, F. L., *Fuzzy Logic Control and Use with MATLAB*, Xi'an Jiaotong University Press, Xi'an, 2002, pp. 2–24 (in Chinese).
- [13] Applebaum, E., Asher, J. B., and Weller, T., "Fuzzy Gain Scheduling for Flutter Suppression in an Unmanned Aerial Vehicle," *Journal of Guidance, Control, and Dynamics*, Vol. 28, No. 6, 2005, pp. 1123–1130. doi:10.2514/1.12662
- [14] Gili, P. A., and Ruotolo, R., "A Neural Gust Alleviation for a Non-Linear Combat Aircraft Model," AIAA Paper 97-3761, 1997.
- [15] Karpel, M., and Moulin, B., "Dynamic Response of Aeroservoelastic Systems to Gust Excitation," *Journal of Aircraft*, Vol. 42, No. 5, 2005, pp. 1264–1272. doi:10.2514/1.6678
- [16] Moulin, B., and Karpel, M., "Gust Loads Alleviation Using Special Control Surfaces," *Journal of Aircraft*, Vol. 44, No. 1, 2007, pp. 17–24. doi:10.2514/1.19876
- [17] Mamdani, E. H., and Assilian, S., "An Experiment in Linguistic Synthesis with a Fuzzy Logic Controller," *International Journal of Man-Machine Studies*, Vol. 7, No. 1, 1975, pp. 1–13. doi:10.1016/S0020-7373(75)80002-2
- [18] Lin, C. L., and Chen, Y. Y., "Design of Fuzzy Logic Guidance Law Against High-Speed Target," *Journal of Guidance, Control, and Dynamics*, Vol. 23, No. 1, 2000, pp. 17–25. doi:10.2514/2.4515